Tectonics

Correspondence to:
S. Marco,
shmulikm@tau.ac.il

Archaeological record of earthquake ruptures in Tell Ateret, the Dead Sea Fault

Ronnie Ellenblum[1], Shmuel Marco[2], Robert Kool[3], Uri Davidovitch[4], Roi Porat[4], and Amotz Agnon[5]

[1]Department of Geography, Hebrew University of Jerusalem, Jerusalem, Israel, [2]Department of Geosciences, Tel Aviv University, Tel Aviv, Israel, [3]Department of Coins, Israel Antiquities Authority, Jerusalem, Israel, [4]Institute of Archaeology, Hebrew University of Jerusalem, Jerusalem, Israel, [5]Institute of Earth Sciences, Hebrew University of Jerusalem, Jerusalem, Israel

Abstract The archaeological Tell Ateret (North Israel), constructed on the active Dead Sea Fault, was intermittently settled for over six millennia. Structures on the Tell that have been offset by earthquake ruptures provide a remarkable record of alternating construction and slip. We excavated the site in order to resolve the geometry and to time the earthquake rupture history back to the earliest settlement. The measurements of faulted archaeological walls are complemented with data from historical documents, numismatic analysis, and geological observations. We report three newly discovered offsets that add to two previously resolved slip events (the 20 May 1202 and 30 October 1759 earthquakes), completing a three millennia archaeoseismic record. The oldest offset measuring at least ~2 m bisected Iron Age IIA fortifications. The second offset, the largest of all five, reaching ~2.5 m, is dated to circa 142 BCE. The third, whose post-Hellenistic date is not determined, is of ~1.5 m, possibly resulting from multiple earthquakes. We constrain the time of the largest offset by a hoard of 45 coins, the latest of which had been minted 143/142 BCE. Indicative pottery and historic texts support the year 143/142 as *terminus post-quem* of the rupture at this site. These observations, together with a new kinematic approach, show uneven slip distribution in time and variable amounts of slip along the Jordan Gorge segment of the Dead Sea Fault. We suggest, based on previous palaeomagnetic measurements, that distributed deformation west of Tell Ateret can explain the apparent missing slip of 4.5 ± 3.5 m since the Hellenistic times.

1. Introduction

Long and precise records of strike-slip surface-rupturing earthquakes are rare, as suitable slip markers are. The shapes of stream channels, the common slip markers in on-fault palaeoseismic studies, are often difficult to resolve precisely. But in the Middle East, the wealth of archaeological structures, in particular along the active Dead Sea Fault (DSF), provides opportunities for on-fault archaeoseismic research that holds the potential for finding sites with offset masonry structures [*Altunel et al.*, 2009; *Haynes et al.*, 2006; *Klinger et al.*, 2000; *Marco*, 2008; *Meghraoui et al.*, 2003; *Niemi et al.*, 2001; *Thomas et al.*, 2007]. Because the original shapes of ancient man-made structures, in particular various types of walls, are well known they provide tight constraints on the deformation. Furthermore, the ages of archaeological artifacts can often be determined with significantly better accuracy than radiocarbon dating of stream channels because of the frequent cultural and political changes in the region.

The study site of Tell Ateret is atop a structural mound that dominates the strategic crossing of River Jordan (Figure 1). The mound is crossed by the Jordan Gorge segment of the DSF. This segment is associated with distributed deformation, expressed as counterclockwise paleomagnetic rotations (11° ± 4°) of 0.9 Ma basalt flows [*Heimann and Ron*, 1993]. Therefore, the displacements recorded by masonry walls in Tell Ateret are expected to show only a part of the total plate motion.

The archaeological strata of the Tell include (bottom to top) Iron Age II fortification, a Hellenistic complex with houses and fortifications, and a medieval Crusader castle called Vadum Iacob (meaning Jacob's Fords). Vadum Iacob forms the most conspicuous remnant with a formidable defense wall and inner structures. The name commemorates the legendary abode of the biblical Patriarch Jacob during the disappearance of his son Joseph [*Ellenblum*, 2003]. The last structure on the Tell is a Mamluk and an Ottoman pilgrimage site with a mosque containing smoking paraphernalia dating the layer to the later to the late Ottoman period (Table 1 provides calendric time spans of archaeological periods).
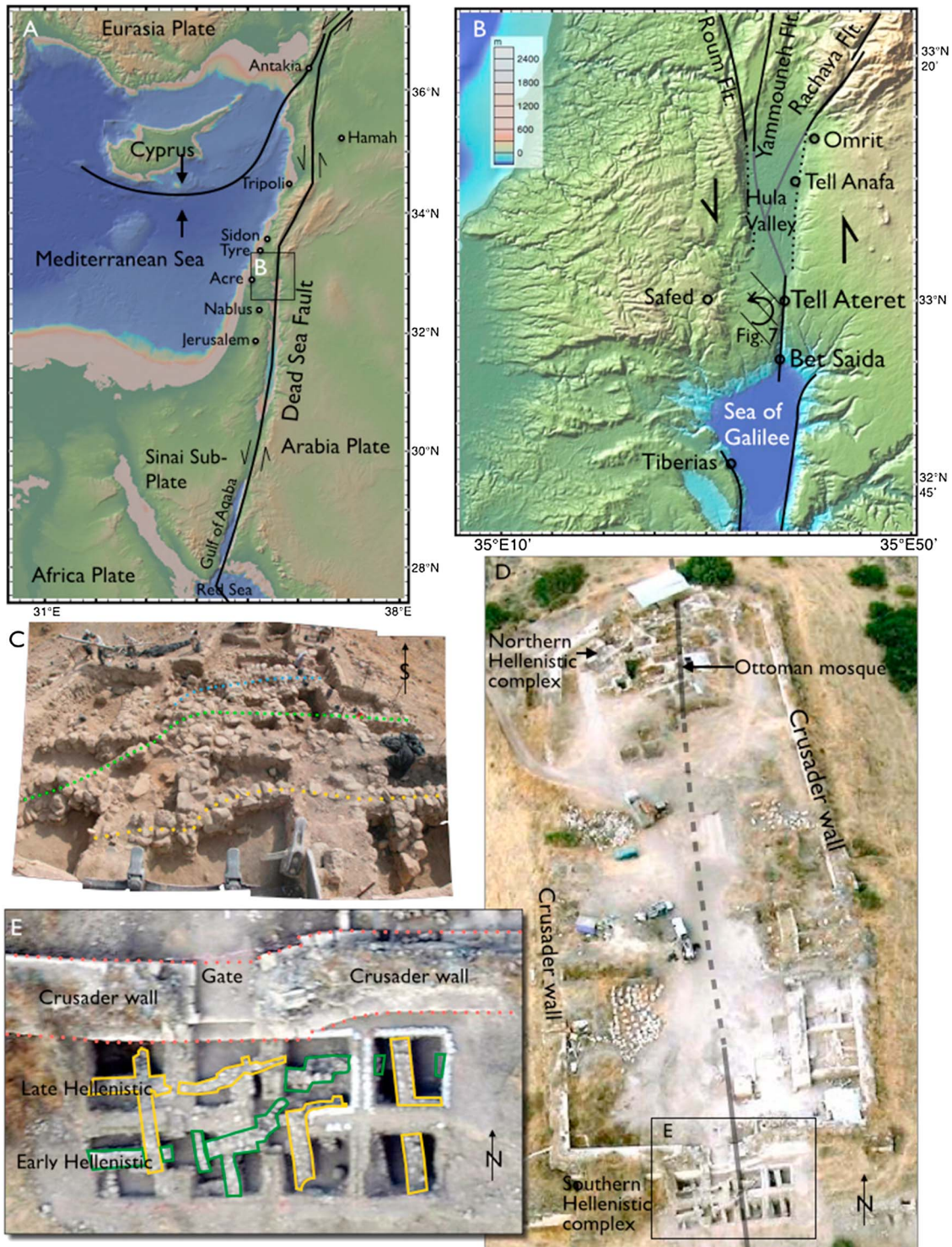
Figure 1. (a) The tectonic plates in the Middle East. Base map: the Global Multi-Resolution Topography (GMRT). (b) Location of Ateret on the trace of the Jordan Gorge Fault between the basins of the Hula and the Sea of Galilee. Solid lines mark strike-slip faults; gray lines mark faults at subsurface according to *Schattner and Weinberger* [2008] and *Politi* [2011]. Dotted lines mark normal faults. Black arrow west of Ateret shows the location of paleomagnetic declinations and geochronology studies of basalt flows that found counterclockwise block rotations about vertical axes of 11.4° ± 4° per million years [*Heimann and Ron*, 1993]. Base map: GMRT. (c) An oblique south looking photomosaic showing the Hellenistic complex during the excavations. The Iron Age wall is marked with blue dots, green dots mark the early Hellenistic wall that we use for measuring displacement, and yellow dots mark a late Hellenistic wall. (d) An oblique north looking air-photo showing Tell Ateret. Gray line marks the DSF. (e) The Hellenistic walls south of the Crusader fortress (pink dotted lines). The dated early Hellenistic walls are highlighted with green lines; late Hellenistic walls with yellow lines.

Table 1. Calendric Time Span of Archaeological Periods in the Middle East

Archaeological Period	Time Span
Bronze Age	3330–1200 BCE
Iron Age I	1200–980 BCE
Iron Age IIA	980–830 BCE
Iron Age IIB-C	830–586 BCE
Persian period	586–333 BCE
Hellenistic period	333–63 BCE
Roman period	63 BCE to 324 CE
Byzantine period	324–638
Early Islamic period	638–750
Abbasid-Fatimid period	750–1099
Crusader period	1099–1187
Ayyubid-Mamluk period	1187–1517
Ottoman period	1517–1917

In our previous work at Tell Ateret we recovered the earthquake history of the last millennium [*Ellenblum et al.*, 1998; *Marco et al.*, 1997]. The most recent event that ruptured on 30 October 1759 bisected the Ottoman mosque. This earthquake was associated with ~0.5 m slip measured both at Tell Ateret and Beit Saida [*Marco et al.*, 2005]. This slip concurs with estimates of M6.6, based on the spatial distribution of the damage of this earthquake, followed less than a month later by a M~7 rupture on the Serghaia-Rachaya branch of the transform [*Ambraseys and Barazangi*, 1989]. Paleoseismic trenching in western Syria identified an eighteenth century CE rupture on that branch [*Gomez et al.*, 2003]. The penultimate earthquake ruptured at dawn of 20 May 1202 CE, when the embattled ruin of the Crusader castle of Vadum Iacob was displaced sinistrally. We measured the displacement of 2.1 m on E-W trending walls of the castle [*Ellenblum et al.*, 1998; *Marco et al.*, 1997] and an aqueduct some 200 m south of the castle [*Agnon*, 2014]. Subtracting ~0.5 m measured on the mosque we obtain 1.6 m for the penultimate rupture. Theses results are corroborated with two buried stream channels in Beit Saida that are displaced 2.2 m [*Marco et al.*, 2005] as well as paleoseismic trench observations of the 1202 earthquake rupture along the Yammouneh Fault in Lebanon [*Daëron et al.*, 2005; *Gomez et al.*, 2003; *Nemer et al.*, 2008]. The slip observed is consistent with earthquake magnitude estimates of M7.5–7.8 based on the damage distribution [*Ambraseys and Melville*, 1988; *Hough and Avni*, 2009]. Historical accounts tell that the 20 May 1202 earthquake shook Syria and the Crusader states. Many cities, including Nablus, Acre, Safed, Tyre, Tripoli, and Hamah, were severely damaged. Rockfalls in Mount Lebanon killed 200 people. Shaking was felt throughout the Mediterranean and Middle East from Sicily to Iraq and from Istanbul to Aswan. The fault rupture is located well within the region of maximum isoseismal zones [*Ambraseys and Melville*, 1988; *Hough and Avni*, 2009; *Sieberg*, 1932].

Here we report results from new excavations in three pre-Crusader strata, comprising dwellings of two superimposed Hellenistic settlements (third to first centuries BCE), possibly identified with the Seleucid fortress of *Pharanx Antiochus*, captured by the Hasmonean King Alexander Jannaeus in 81 BCE [*Ma'oz*, 2013], and an underlying Iron Age IIA (circa 980–830 BCE) defense wall. The present research stage is aimed at extending the record of displacements back to the Iron Age, testing the completeness of the historical earthquake catalogues for the pre-Crusader period for this region, and use the fine details of the geometry preserved in the displaced walls for imposing constraint on the distribution of slip within the fault zone. The well-exposed masonry that exhibits clear predisplacement geometry enables precise determination of the slip, which allows us a kinematic analysis that explains the strain partitioning along this section of the DSF.

In the following sections we describe the deformed structures that we exposed underneath the Crusaders strata.

2. Deformed Hellenistic Structures

Hellenistic structures have been excavated south of the Crusader curtain wall, both in the north and in the south of Tell Ateret (Figure 1d). The Northern Hellenistic complex comprises massive fortifications showing damage beyond ability to determine the original masonry at the present level of exposure. The southern complex ("Area E") allows tracing of walls across the fault zone. Two building phases are discernible in this excavated Hellenistic compound with crosscutting relations that determine their temporal relations. The walls of both phases are deformed and truncated at the fault immediately south of the faulted Crusader wall. The foundation walls of the early phase are 60–80 cm thick, made of non-cemented local basalt and limestone cobbles. The walls of the second phase are different: the cobbles
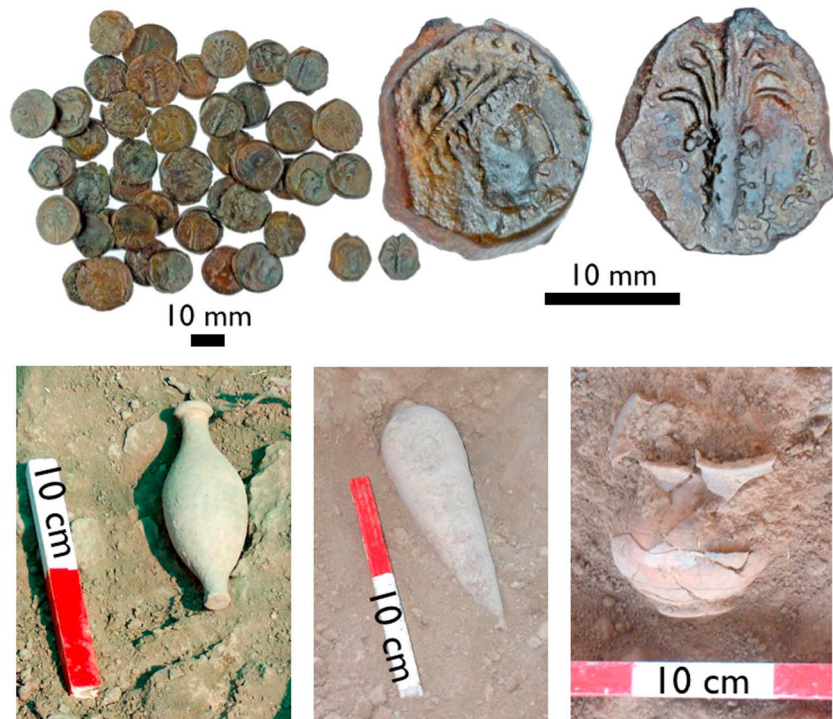
Figure 2. Top left: A hoard of 45 small Seleucid "palm tree" bronze coins. These coins were the smallest bronze denomination available at the time and widely used for small cash transactions in Seleucid-controlled Palestine. The diameters of the coins range between 14 and 16 mm. Top center: Diademed head of the Seleucid ruler Demetrius II Nicator, (first reign 146–138 BCE), set in dotted border. Top right: Palm tree, with curved Greek inscription "[Basi]leos [Demetriou]." The date is in Greek numerals, left and right of the tree: $o - \rho$ (=year 170 of the Seleucid Era), which is 143/142 BCE. Bottom: Indicative Hellenistic period vessels.

are cemented, the foundations are deeper—over 1.5–2 m below the foundations of the earlier phase, and the width of the walls is 50 cm. The walls of the earlier phase are invariably straight along 20 m except for within the fault zone, where they are crooked left laterally. Heaps of cobbles at the bottom of the walls, which have fallen from the upper parts of the early phase walls, buried indicative artifacts including candles, vessels, cooking pots, decorated fishplates, and relief bowls, as well as imported Hellenistic wares and a hoard of coins (Figure 2). All these findings unambiguously belong to the Hellenistic period. The most special finding is a hoard of 45 small bronze coins buried within the debris of the older walls. A numismatic analysis of the 32 well-preserved datable coins limits the range of the hoard to 150s–140s BCE. The latest dated coin, shown in Figure 2, was minted in 143/142 BCE. About 60% of the coins cluster close to this date.

2.1. Interpretation

The context of the coin hoard in the debris at the base of the early Hellenistic wall is consistent with a scenario of sudden collapse of the wall, possibly triggered by an earthquake. The types and the arrangement of the walls indicate that the two successive construction periods were separated by a destruction event within the Hellenistic period, which left a considerable amount of debris along the fault. Based on the stratigraphy and lateral displacement, we attribute the termination of the older phase to an earthquake that tore apart the earlier phase during the second century BCE. The latest dated coin in the hoard (Figure 2), minted in 143/142 BCE, provides a lower bound for the date of this earthquake, after which the late Hellenistic walls were built. In another two-phase Hellenistic settlement some 20 km north of Ateret-Tell Anafa, an abrupt termination of a well-developed settlement with elaborate construction [*Herbert*, 1993], may be re-interpreted as a result of an earthquake destruction. *Heimann and Ron* [1987] interpreted the hill of Tell Anafa as a push-up structure that was formed where the Rachaya fault trace makes a right jog.
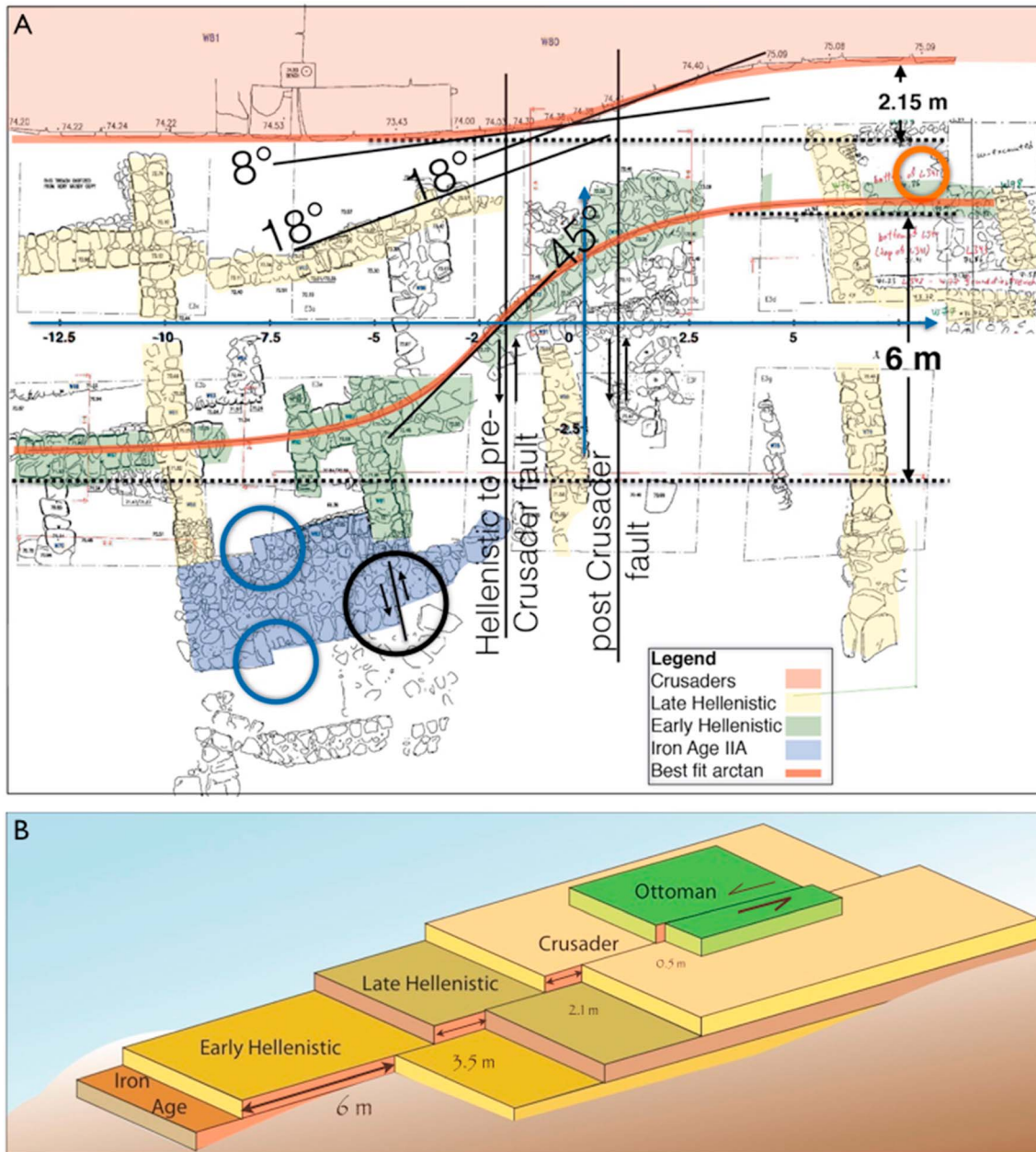
Figure 3. (a) Map of the excavation in the southern part of Tell Ateret (see Figure 1e for location) showing the best fit curves in red, axes in blue, which we use for the kinematic analysis (equation (2)). In the analysis of deformation above buried faults the walls are assumed originally linear and trending E-W, perpendicular to faults. Angles denote β_{max}, rotation relatively to E-W. Faults are assumed parallel. Ruptures on the same fault are assumed to reach upward (unlock) to the same depth. Orange circle shows the location of the bronze coin hoard. Blue circles show inset-offset architecture in the Iron Age wall. Black circle shows a 70 cm left-lateral offset of the Iron Age curtain wall that predates the Hellenistic structures. This is a part of the larger offset and bending that exceeds 8 m. Measured elevations are denoted with small digits (m above sea level). (b) A schematic illustration of the archaeological strata at Tell Ateret offset by the DSF. The older the strata the larger the offset.

The Hellenistic walls are bent immediately south of the faulted Crusader wall. Reconstruction of the early wall to its original straight disposition requires about 6 m (Figure 3). The later wall (highlighted yellow), dated to the late second-first century BCE, is exposed along ~8 m. It is also curved leftward at the center by about 20°. The builders of the Crusader wall destroyed the eastern segment of the late Hellenistic wall, making direct measurement of the displacement impossible. The latest Hellenistic coin excavated from the late phase of construction is dated to 65/64 BCE, indicating desertion of the site during the mid-first century BCE. The latter date coincides with the year of an historic earthquake for which the geographical extent is debated [*Karcz*, 2004], but a seismite that matches this age is found within the Dead Sea
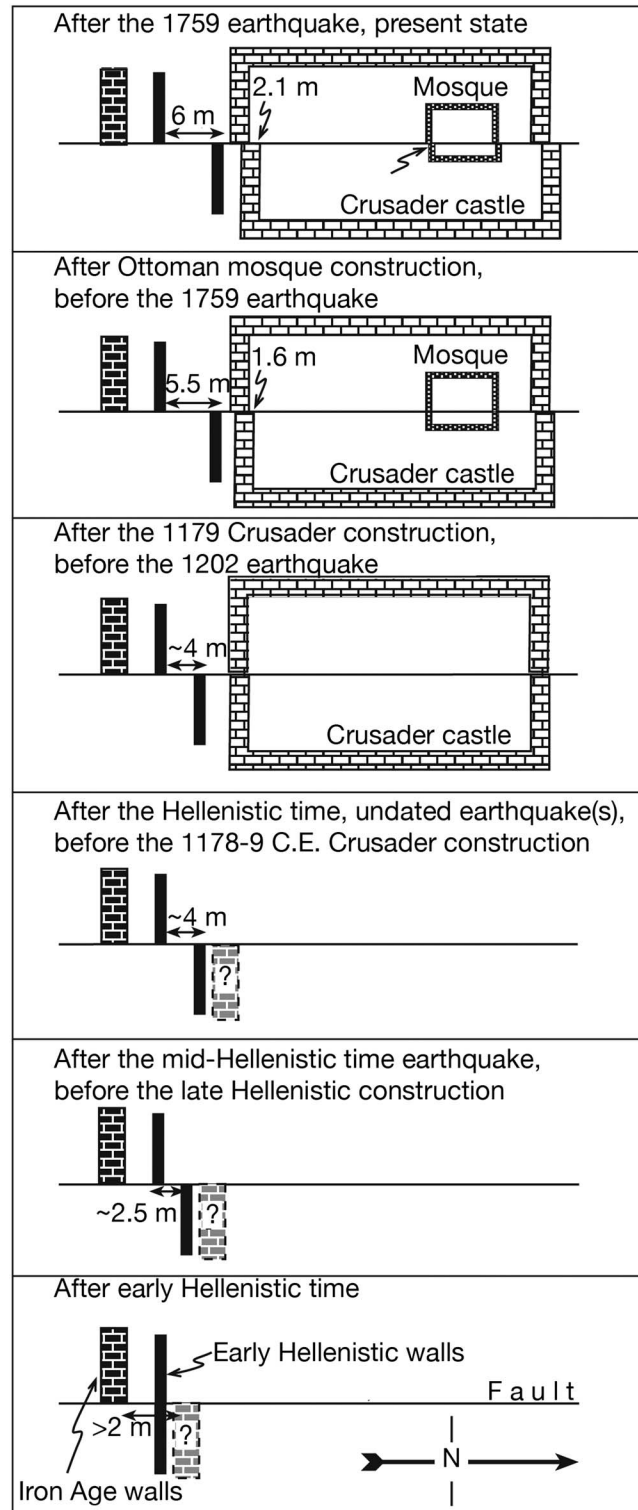
Figure 4. Schematic illustration of the stages of slip accrual (values are rounded) in the Ateret structures, timeline from bottom to top.

sediments [*Kagan et al.*, 2011; *Ken-Tor et al.*, 2001]. The settlement was subsequently renewed only during the twelfth century CE, when the Crusader castle of Vadum Iacob was constructed [*Ellenblum*, 2003].

3. Iron Age Structures

To the South and partially beneath the Hellenistic ruins we unearthed the remains of a 2.4 m wide wall dated to the Iron Age IIA (circa 980–830 BCE). The preliminary dating is based on architectural and pottery typologies: the style of the fortification, built as an "inset-offset" wall (a type of defensive wall that has alternating sections set protruding or receding; Figure 3), with dressed limestone blocks in the inner and outer joints of each inset-offset; a typical Iron Age IIA cooking pot unearthed from the inner foundation trench of the wall. The considerable width of the wall and the absence of other architectural remains to the south of it (albeit pottery remains are found some 30 m south of the fort) suggest that this is the outer Iron Age fortification wall. The area north of the wall was not excavated below the Hellenistic layers; therefore, the extent of this settlement and its characteristics are not determined yet.

The Iron Age IIa wall is truncated at the same fault zone that truncates the Hellenistic walls. We excavated the area east of the fault zone down to the basaltic bedrock, 16 m to the east and 8 m to the north, up to the Crusader wall. Despite the extensive excavations, no continuation of the Iron Age IIa wall was exposed and no Iron Age-related potshards could be detected east of the fault.

3.1. Interpretation

The absence of an Iron Age wall east of the fault (and south of the Crusader wall), together with rich pottery remains some 30 m farther south, leads us to conclude that the wall was displaced at least 8 m northward, possibly to where the Crusaders had built their fortress. Six meters out of these 8 m took place after the early Hellenistic period. Therefore, at least 2 m of slip occurred in an unknown number of events during the first millennium BCE prior to the 142 BCE earthquake (Figure 4).
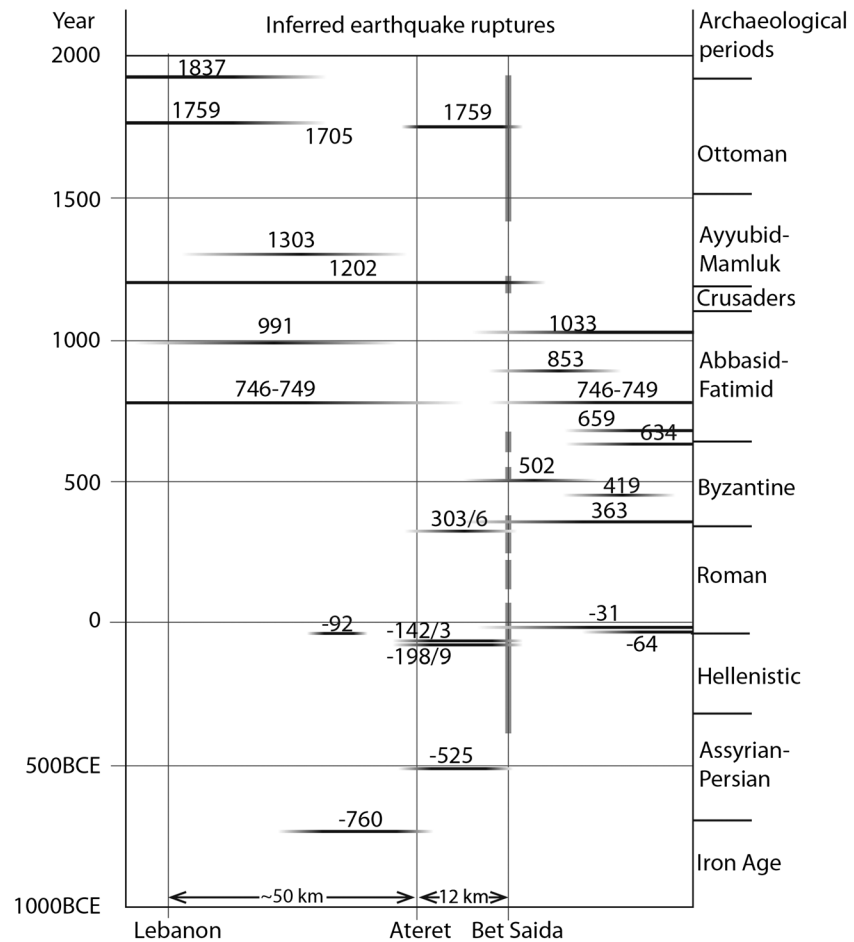
Figure 5. Time (vertical axis) and location (horizontal axis) of historical earthquakes reported in the vicinity of Ateret shown as horizontal bars with gradual fading to illustrate uncertainty in location [after *Agnon*, 2014; *Marco and Klinger*, 2014]. Vertical gray bars represent ranges of ^{14}C ages of slip events from the Bet Saida paleoseismic trenches [*Marco et al.*, 2005; *Wechsler et al.*, 2014].

Field evidence and reports on earthquakes between the Hellenistic and the Crusader periods in the region had been reported (Figure 5) but are difficult to resolve at Ateret because the site had been abandoned during this time. Subtracting 2.15 m post-Crusaders slip from 6 m post Hellenistic slip shows that about 3.8 m of slip occurred in that interval. The historical accounts suggest that candidate earthquakes occurred in the fourth century, the mideighth century, and the late tenth century. Other nearby archaeological sites that exhibit earthquake damage including the Roman Temple II of Omrit, 23 km north of Ateret, are interpreted as showing earthquake damage during the fourth century CE [*Agnon*, 2014; *Overman*, 2008; *Stoehr*, 2011], and "a second earthquake in the middle of the eighth century CE appears to have brought about the final destruction of the site" [*Stoehr*, 2011].

Six slip events recorded on faulted stream channels in the Bet-Saida Valley (12 km south of Ateret; Figure 1) are constrained by [14]C [*Wechsler et al.*, 2014] and correlated to historic earthquakes between the midsecond century BCE and seventh century CE that are listed in the catalogues [*Ambraseys*, 2009; *Guidoboni et al.*, 1994; *Sbeinati et al.*, 2005]. The estimated locations of historical earthquakes in the vicinity of Ateret as interpreted from historical texts and paleoseismic research (Figure 5) illustrate the contribution of the findings at Ateret toward ground truth testing of the ancient texts; they underscore which earthquakes still require verification.

4. Kinematic Analysis

Four displaced E-W trending walls in the southern perimeter of the Tell enable the estimation of slip and deformation. Where exposed away of the fault zone the intact walls trend E-W, respecting the southern slope

of the hill. Assuming that the walls were originally built along straight E-W lines, their present curvy shapes at the fault zone record the cumulative displacements of recurring deformation events. This is consistent with the observation of older and more curved walls (Figure 3). We determine the sequence of displacements by subtracting the later displacements from the earlier ones (Figure 4). The straight undeformed wall segments away from the fault indicate that the width of the excavation spans the entire fault zone and enables quantification of the deformation.

The Crusader walls show bending on the fault zone, suggesting that the fault manifests as a distributed shear zone spanning about 7–8 m (Figure 1). In our previous work at the site [*Ellenblum et al.*, 1998] we show discrete shear planes near the surface but because the walls are made of large ashlars they bend with an arc-tangent shape. In order to estimate slip at some depth we model its effect on the walls at the surface. We note the similarity between the southern Crusader wall plan and the function arctangent (Figure 3). This suggests deformation over a buried dislocation (compare with the related problem of interseismic deformation in *Savage and Burford* [1973]). At the surface above a vertical (laterally infinite) fault in a uniform elastic half-space this solution takes the form

$$u(x) = (2u^0/\pi)\arctan(x/h),\qquad(1)$$

where u is the displacement parallel to the fault, x is the horizontal distance from the fault trace, and h is the depth to the top of the moving fault. u^0 is half the far-field displacement approaching the slip of the fault on each block at depth. For geodetically monitored faults, h is in the order of 10 km, representing the seismogenic crust that ruptures during large earthquakes [*Even-Tzur and Hamiel*, 2011; *Masson et al.*, 2015]. Here h is only of order meter, representing the thickness of a surface layer that relaxes plastically following seismic rupture up to shallow depth.

To test the similarity between the trace of the deformed wall and an arctangent solution (equation (1)) we use two measurements for constraining the solution and compare the plots (Figure 3a, red curve over edge of pink wall): the far-field half-offset u^0 and the angle of maximum rotation of ashlars at the fault zone β_{max}. The offset of the walls at the corners reaches 2.1 m where the rotation seems negligible [*Marco et al.*, 1997]. For β_{max} we measure $21° \pm 0.5°$. This angle is given by differentiating equation (1):

$$\tan(\beta) = 2u^0 h/\left[\pi(h^2 + x^2)\right]\qquad(2)$$

The maximum value of β is given at $x = 0$ (inflection point):

$$\beta_{max} = \arctan\left[2u^0/(\pi h)\right]\qquad(3)$$

from which h is extracted by

$$h = 2\,u^0/\left[\pi\,\tan(\beta_{max})\right]\qquad(4)$$

The striking similarity between the contours of the Crusader defense wall and the solution (1) suggests that the two post-Crusader events of 1202 and 1759 CE ruptured to the near-surface precisely along the same geometry, well represented by a buried half plane. As a result, the cumulative displacement of the two events u amounts to 2.1 m. The depth to the rupture is estimated in two ways: first we measure the angles between the ashlar side and the $090° = 270°$ (E-W) bearing that represents the far-field prerotation state, on an archaeological plan (Figure 6a). These angles increase from nil outside the fault zone to a maximum of 18°. At 9–10 m west of the axis the angles become slightly negative, perhaps responding to the rotation of the large intact block of three ashlars neighboring on the east. Substituting in equation (4) we get $h = 2.06$ m. As a check on the fit we plot the function $\tan(\beta(x))$ and compare to the observed for different values of h. A range of 1.95 ± 0.11 m gives satisfactory fits (corresponding to $\beta_{max} = 19° \pm 1°$; Figure 6). We chose to fit to the angles despite the challenge of fitting to a gradient of the displacement field: the rotations are readily measured from the plan at subdegree accuracy and account for the rigidity of the ashlars.

In the case of migration of the rupture half plane between consecutive intervals the cumulative displacement should obey

$$u(x) = (2/\pi)\,\Sigma_i u^0{}_i \arctan\left[(x - x_i)/h_i\right],\qquad(5)$$

where the subscript i denotes a specific time interval in which rupture events follow a congruent geometry around a fault plane satisfying $x = x_i$.
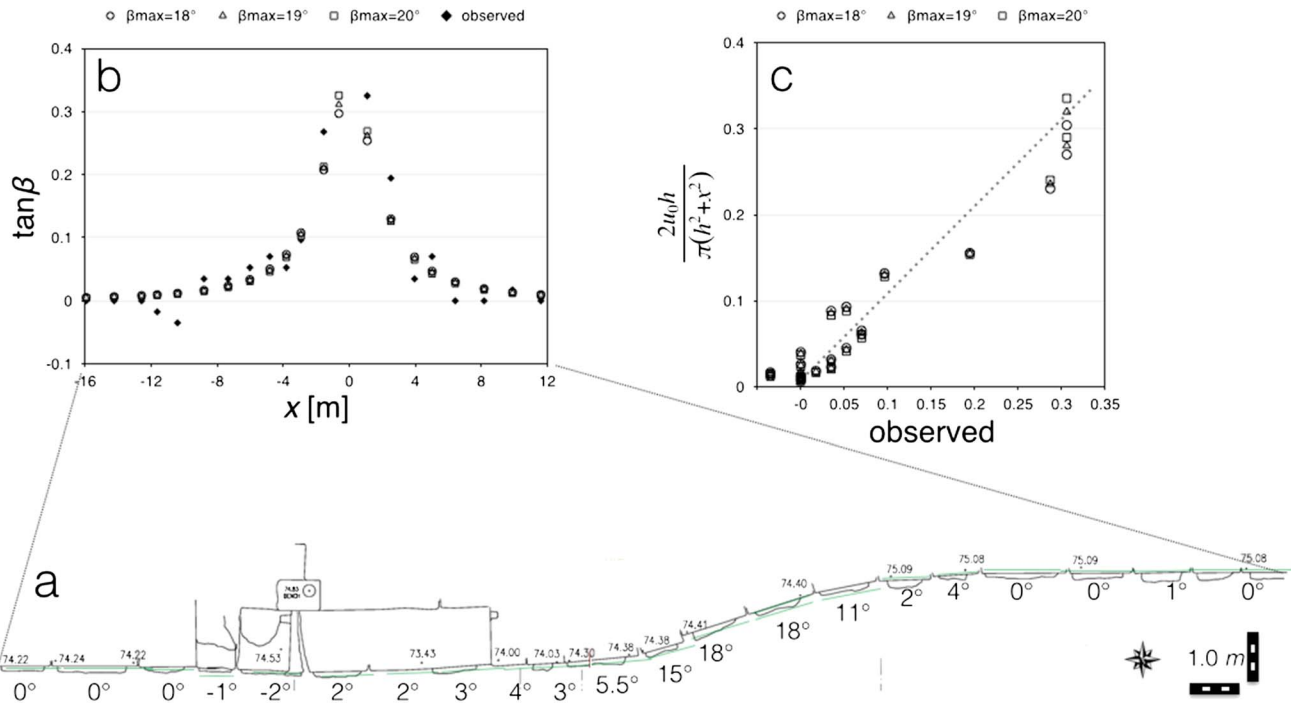
Figure 6. Constraints of the depth to rupture h. (a) Archaeological plan of the southern face of the Crusader curtain wall with measured angles of rotations β relatively to 090°–270° (E-W). (b) Tangent of observed $\beta(x)$ compared with calculated by equation (2) for various values of β_{max}. (c) Correlation between values of tangent, the observed rotation angle β (horizontal axis) and calculated by equation (2) for various values of β_{max} (vertical axis). Measured elevations are indicated with small digits ranging from 73.4–75.09 (m above sea level) on the wall map.

We proceed by subtraction of the dislocation field of the second millennium CE ($u_1^0 = 2.1$ m) from the profile of the early Hellenistic wall and then resolving the latter by the remnants of the late Hellenistic wall. This wall is better preserved than the late Hellenistic wall and allows a more complete geometrical analysis. Table 2 presents coefficients for the solution of three incremental slip events ($i = 1,3$ in equation (5)), where for the two earlier ruptures the fault does not change ($h_2 = h_3$; $x_2 = x_3$).

The early Hellenistic wall fits a two-term sum of the form (equation (5)), with $u_2^0 \sim 4$ m. This displacement is centered about a surface rupture $x = x_2 = 2.7$ m $+ x_1$ (west of the post-Crusader rupture: Figure 3). The maximum rotation angle for the Hellenistic to pre-Crusader phase is around 45°, but it includes ~8° of post Crusader rotation (Figure 6). Considering the additive shear, we calculate $\beta_{max} = 41° \pm 3°$ and $h_2 = 1.5 \pm 0.1$ m. The resulting solution (equation (5)) shows that the Hellenistic exposures do not reach the far field asymptote, and a pre-Crusader slip of 4.5 is required.

To resolve these 4.5 m of two Hellenistic to pre-Crusader events we assume that all slip events rupture the same fault with the same thickness for the overlying zone of distributed deformation, so we measure the rotation of the late Hellenistic wall just west of the reconstructed trace as $18° \pm 1°$ (Figure 6). Correcting for post-Crusader shear we obtain $8° < \beta_{max} < 13°$. This ranges between a quarter and third of the shear recorded in the early Hellenistic prior to Crusader construction. The corresponding displacement of the post early Hellenistic wall is 3.2 ± 0.2 m during the Hellenistic Period and $\sim 1.3 \pm 0.2$ m between the late Hellenistic and the Crusader period. The uncertainties calculated here are minimal due to the multitude of assumptions.

Table 2. Coefficients for the Solution of Incremental Slip Events (Equation (5))

i	Pre-	Post-	$u^0\ i$ m	$h\ i$ m	β Max Observed	β Max Corrected
1	Present	Crusader	2.1	1.7–1.8	21° ± 0.5°	21° ± 0.5°
2	Crusader	Late Hellenistic	1.2 ± 0.2	1.6 ± 0.1	19° ± 2°	10.5° ± 2.5°
3	Late Hellenistic	Early Hellenistic	3.2 ± 0.2	1.6 ± 0.2	45° ± 2°	41° ± 3°
4	Early Hellenistic	Iron Age IIA	≥1.5	?	>45°	>41°

However, one should bear in mind that our implicit assumption on originally straight linear wall segments may be more justified than equivalent assumptions in traditional paleoseismic data.

5. Discussion

A decade of excavations at Tell Ateret has yielded unprecedented precision for estimates of a series of consecutive offsets, with uncertainties below 0.5 m. Since the Iron Age IIa Period almost three millennia ago, the total left-lateral slip amounts to at least 8 m. During the earliest interval (post-Iron Age IIa and pre-Hellenistic) the fault has slipped 2 m or more; the mid-Hellenistic rupture generated about 2.6 m slip; the third post-Hellenistic pre-Crusader slip episode amounted to 1.3 m slip. These three ruptures now complement two previously noted slips at the site, 1.6 m and 0.5 m, which ruptured during earthquakes in 1202 CE and 1759, respectively [*Ellenblum et al.*, 1998]. The calculated average slip rate in the last three millennia is 2.6 mm/yr (assuming all the slip is localized at Ateret) or higher (if other unrecognized strands take part of the slip). This is considerably lower than the GPS lower margin 4.9 ± 1.4 mm/yr [*Even-Tzur and Hamiel*, 2011; *Le Beon et al.*, 2008; *Masson et al.*, 2015; *Sadeh et al.*, 2012] and the longer-term geologic slip rates of ~5 mm/yr [e.g., *Marco and Klinger*, 2014] and 7 mm/yr reported for farther north in Syria [*Meghraoui et al.*, 2003]. Extrapolating the GPS measurements to the last 22 centuries (the Hellenistic period), the plates should have accumulated 10.5 ± 3 m of differential displacement. The discrepancy between the archaeological measurements (6 ± 0.5 m) and the respectively longer and shorter-term geodetic and geologic rates amounts to 4.5 ± 3.5 m, indicating distributed and possibly temporally uneven slip distribution.

The relative displacement between the tectonic plates, estimated from far-field short-term GPS displacements, is likely to be distributed between the main fault at Tell Ateret and secondary strands. An estimate for the displacement distributed west of the main fault is given from analysis of rotations about vertical axes, derived from paleomagnetic declinations and geochronology of basalt flows of 11.4°±4° per million years counter clockwise [*Heimann and Ron*, 1993]. The sinistral displacement ū associated with this rotation is ū=w(cotanθ_i-cotanθ_f). The 11°±4° cumulative rotations over a 6±0.5-km-wide zone may be associated with sinistral displacement between minimum ū=1.7±0.1 km and maximum ū=4.4±0.3 km. Assuming a constant rate, this rotation can account for sinistral slip between 3.4 m and 8.8 m during the last two millennia since the Hellenistic period, in addition to the 6 m slip observed at Ateret. Hence, the slip discrepancy since the Hellenistic times could be accounted for by rigid block rotations.

The accommodation of plate motions by both block rotations and occasional slip during large earthquakes implies that only part of the total strain is released during each process. Although spatial distribution of deformation can accommodate the entire discrepancy between our archaeological measurements and geodetic and geologic rates, the time scales of the observations are very different, and we do not know the plastic fraction of the ongoing rotation. We should consider the possible role of uneven temporal distribution of slip over several millennia, as this has implications for predicting the largest possible earthquake. This holds particularly for the DSF, where long-term clustering of earthquakes has been inferred [*Agnon*, 2014; *Marco et al.*, 1996]. If a slip deficit of 4.5 ± 3.5 m has accumulated in the last two millennia, we may expect an earthquake of magnitude 7.5 or more to release the elastic energy [*Wells and Coppersmith*, 1994] unless part of the plate motions is distributed over wider fault zone. The considerable uncertainty in predicting the maximum magnitude of such an earthquake underscores the need for more accuracy and precision in geodetic and geological data.

Although the offsets at any single site represent the release of strain at that point we can argue that the variation of slip from 0.5 m of the 1759 earthquake to over 1.5 m in earlier earthquakes is incompatible with a characteristic slip model. For comparison, a palaeoseismic trench study at the Gerede segment of the North Anatolian fault reveals four slip events that exhibit quasiperiodicity and characteristic slip per event of 5.0 ± 0.8 m [*Kondo et al.*, 2010], and analysis of high-resolution satellite data shows that the ruptures on the Fuyun Fault in China obey a characteristic slip model [*Klinger et al.*, 2011]. In contrast, [*Weldon et al.*, 2004], who have recorded prehistoric earthquakes along the San Andreas Fault, find that slip per event at Wrightwood varied from 0.7 m to 7 m in the past 1500 years. They show that the earthquake occurrence in the past 6000 years is slightly more ordered than random and has a notable cluster of events and that slip associated with an earthquake is not well predicted by the interval preceding it. Analysis of high-resolution topographic data shows that slip at the Carrizo segment of the San Andreas Fault prior to the 1857
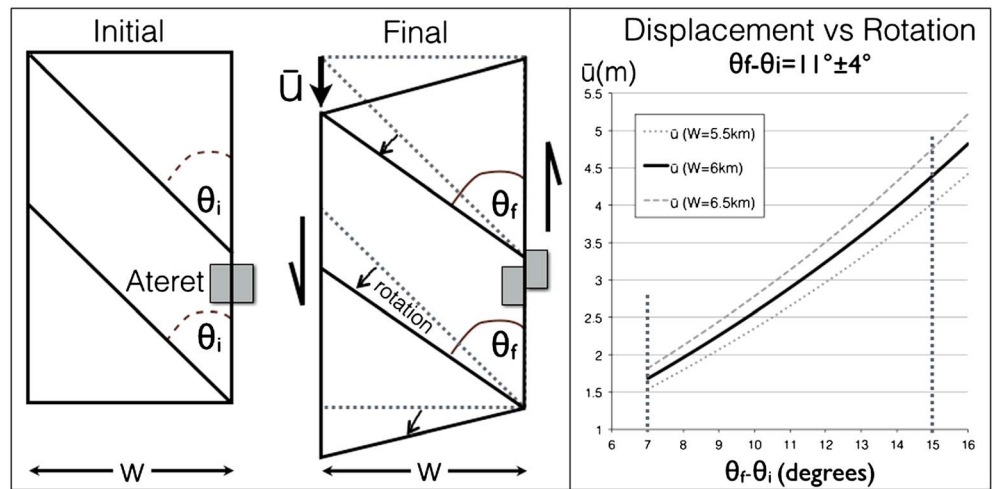
Figure 7. A schematic illustration showing how the measured paleomagnetic rotations of the faulted 1 Ma old flood basalt west of Ateret can take part of the sinistral motion on the DSF. The sinistral displacement $\bar{u}$ is $\bar{u} = w(\cot\theta_i - \cot\theta_f)$. Hence, the $11° \pm 4°$ cumulative rotations over the last 1 Ma [*Heimann and Ron*, 1993], over a 6 ± 0.5 km wide zone may be associated with sinistral displacements between minimum $\bar{u} = 1.7 \pm 0.1$ km and maximum $\bar{u} = 4.4 \pm 0.3$ km. Assuming constant rate, these rotations can account for sinistral slip between 3.4 m and 8.8 m during the last two millennia, in addition to the 6 ± 0.5 m slip observed at Ateret.

earthquake occurred in earthquake clusters with cumulative slip of ~5 m [*Zielke et al.*, 2010]. One important difference to note is that Ateret is located between two pull-apart basins with complex fault geometry, whereas the examples from the North Anatolian Fault, the Fuyun Fault, and the San Andreas Fault are from long, relatively simple fault geometry. Hence, additional sites with longer palaeoseismic records are required to definitively outline the earthquake history of the DSF.

6. Conclusions

At least 8 m of slip have accumulated along the Jordan Gorge segment of the DSF after the construction of the Iron Age walls at Ateret. Younger walls of the early Hellenistic period are offset 6 m, Crusader fortress walls are offset 2.15 m, and an Ottoman mosque is offset 0.5 m. One slip event, evident in the displaced walls of an early Hellenistic building, postdates a hoard of coins recovered from the rubble, the latest of which was minted in 143/142 BCE. Although an earthquake from this time is mentioned in the historical earthquake catalogues, its source was hitherto unknown. About 3.8 m of slip took place between the Hellenistic and the Crusader periods and additional 2.15 m occurred after the Crusader period. The average slip rate in the last three millennia in the Jordan Gorge segment is 2.6 mm/yr, considerably lower than the ~5 mm/yr relative plate velocity determined by geodetic and geologic observations. We suggest that the remaining slip may be accommodated by distributed deformation or by elastic loading that will be released in future earthquakes. We estimate the accumulated slip deficit at 4.5 ± 3.5 m, which future earthquake(s) and possible distributed deformation within a wide fault zone will release (Figure 7). The uneven slip distribution in time, and the variable amounts of slip are incompatible with a characteristic earthquake model for the seismicity of this region.

References

Agnon, A. (2014), Pre-instrumental earthquakes along the Dead Sea Rift, in *Dead Sea Transform Fault System: Reviews*, vol. 6, edited by Z. Garfunkel, Z. Ben-Avraham, and E. Kagan, pp. 207–261, Springer, Netherlands.

Altunel, E., M. Meghraoui, V. Karabacak, S. H. Akyuz, M. Ferry, C. C. Yalciner, and M. Munschy (2009), Archaeological sites (Tell and Road) offset by the Dead Sea Fault in the Amik Basin Southern Turkey, *Geophys. J. Int.*, *179*(3), 1313–1329.

Ambraseys, N. N. (2009), *Earthquakes in the Mediterranean and Middle East: A Multidisciplinary Study of Seismicity up to 1900*, 947 pp., Cambridge Univ. Press, Cambridge.

Ambraseys, N. N., and M. Barazangi (1989), The 1759 earthquake in the Bekaa valley: Implications for earthquake hazard assessment in the eastern Mediterranean region, *J. Geophys. Res.*, *94*(B4), 4007–4013, doi:10.1029/JB094iB04p04007.

Ambraseys, N. N., and C. P. Melville (1988), An analysis of the eastern Mediterranean earthquake of 20 May 1202, in *Historical Seismograms and Earthquakes of the World: San Diego*, edited by W. K. H. Lee, H. Meyers, and K. Shimazaki, pp. 181–200, Academic Press, Calif.

Daëron, M., Y. Klinger, P. Tapponnier, A. Elias, E. Jacques, and A. Sursock (2005), Sources of the large AD 1202 and 1759 Near East earthquakes, *Geology*, *33*(7), 529–532.

Ellenblum, R. (2003), Frontier activities: The transformation of a Muslim sacred site into the Frankish Castle of Vadum Iacob, *Crusades*, *2*, 83–97.

Ellenblum, R., S. Marco, A. Agnon, T. Rockwell, and A. Boas (1998), Crusader castle torn apart by earthquake at dawn, 20 May 1202, *Geology*, *26*(4), 303–306.

Even-Tzur, G., and Y. Hamiel (2011), Geodetic study of crustal deformation across the Dead Sea Fault system in the Jordan Gorge area Northern Israel, *Isr. J. Earth Sci.*, *58*(3), 193–201.

Gomez, F., M. Meghraoui, A. N. Darkal, F. Hijazi, M. Mouty, Y. Suleiman, R. Sbeinati, R. Darawcheh, R. Al-Ghazzi, and M. Barazangi (2003), Holocene faulting and earthquake recurrence along the Serghaya branch of the Dead Sea fault system in Syria and Lebanon, *Geophys. J. Int.*, *153*(3), 658–674.

Guidoboni, E., A. Comastri, and G. Traina (1994), *Catalogue of Ancient Earthquakes in the Mediterranean Area up to the 10th Century*, 504 pp., Istituto Nazionale di Geofisica, Bologna.

Haynes, J. M., T. M. Niemi, and M. Atallah (2006), Evidence for ground-rupturing earthquakes on the Northern Wadi Araba fault at the archaeological site of Qasr Tilah, Dead Sea Transform fault system Jordan, *J. Seismol.*, *10*(4), 415–430.

Heimann, A., and H. Ron (1987), Young faults in the Hula pull-apart basin, central Dead Sea transform, *Tectonophysics*, *141*, 117–124.

Heimann, A., and H. Ron (1993), Geometric changes of plate boundaries along part of the northern Dead Sea Transform: Geochronologic and paleomagnetic evidence, *Tectonics*, *12*(2), 477–491, doi:10.1029/92TC01789.

Herbert, S. (1993), Tel Anafa, in *New Encyclopedia of Archaeological Excavations in the Holy Land*, vol. 1, edited by E. Stern, pp. 58–61, Israel Exploration Society and Carta, Jerusalem.

Hough, S. E., and R. Avni (2009), The 1170 and 1202 CE Dead Sea Rift earthquakes and long-term magnitude distribution of the Dead Sea Fault Zone, *Isr. J. Earth Sci.*, *58*(3–4), 295.

Kagan, E., M. Stein, A. Agnon, and F. Neumann (2011), Intrabasin paleoearthquake and quiescence correlation of the late Holocene Dead Sea, *J. Geophys. Res.*, *116*, B04311, doi:10.1029/2010JB007452.

Karcz, I. (2004), Implications of some early Jewish sources for estimates of earthquake hazard in the Holy Land, *Ann. Geophys.*, *47*(2–3), 759–792.

Ken-Tor, R., A. Agnon, Y. Enzel, S. Marco, J. F. W. Negendank, and M. Stein (2001), High-resolution geological record of historic earthquakes in the Dead Sea basin, *J. Geophys. Res.*, *106*(B2), 2221–2234, doi:10.1029/2000JB900313.

Klinger, Y., J. P. Avouac, L. Dorbath, N. Abou-Karaki, and N. Tisnerat (2000), Seismic behaviour of the Dead Sea Fault along Araba Valley, Jordan, *Geophys. J. Int.*, *142*, 769–782.

Klinger, Y., M. Etchebes, P. Tapponnier, and C. Narteau (2011), Characteristic slip for five great earthquakes along the Fuyun fault in China, *Nat. Geosci.*, *4*(6), 389–392.

Kondo, H., V. Özaksoy, and C. Yıldırım (2010), Slip history of the 1944 Bolu-Gerede earthquake rupture along the North Anatolian fault system: Implications for recurrence behavior of multisegment earthquakes, *J. Geophys. Res.*, *115*, B04316, doi:10.1029/2009JB006413.

Le Beon, M., Y. Klinger, A. Q. Amrat, A. Agnon, L. Dorbath, G. Baer, J. C. Ruegg, O. Charade, and O. Mayyas (2008), Slip rate and locking depth from GPS profiles across the southern Dead Sea Transform, *J. Geophys. Res.*, *113*, B11403, doi:10.1029/2007JB005280.

Ma'oz, Z. U. (2013), A Note on Pharanx Antiochus', *Isr. Explor. J.*, *63*(1), 78–82.

Marco, S. (2008), Recognition of earthquake-related damage in archaeological sites: Examples from the Dead Sea fault zone, *Tectonophysics*, *453*, 148–156, doi:10.1016/j.tecto.2007.04.011.

Marco, S., and Y. Klinger (2014), Review of on-fault palaeoseismic studies along the Dead Sea Fault, in *Dead Sea Transform Fault System: Reviews*, vol. 6, edited by Z. Garfunkel, Z. Ben-Avraham, and E. J. Kagan, pp. 183–206, Springer, Dordrecht.

Marco, S., M. Stein, A. Agnon, and H. Ron (1996), Long term earthquake clustering: A 50,000 year paleoseismic record in the Dead Sea Graben, *J. Geophys. Res.*, *101*(B3), 6179–6192, doi:10.1029/95JB01587.

Marco, S., A. Agnon, R. Ellenblum, A. Eidelman, U. Basson, and A. Boas (1997), 817-year-old walls offset sinistrally 2.1 m by the Dead Sea Transform Israel, *J. Geodyn.*, *24*(1–4), 11–20.

Marco, S., T. K. Rockwell, A. Heimann, U. Frieslander, and A. Agnon (2005), Late Holocene slip of the Dead Sea Transform revealed in 3D palaeoseismic trenches on the Jordan Gorge segment, *Earth Planet. Sci. Lett.*, *234*(1–2), 189–205, doi:10.1016/j.epsl.2005.01.017.

Masson, F., Y. Hamiel, A. Agnon, Y. Klinger, and A. Deprez (2015), Variable behavior of the Dead Sea Fault along the southern Arava segment from GPS measurements, *C. R. Geosci.*, doi:10.1016/j.crte.2014.11.001.

Meghraoui, M., et al. (2003), Evidence for 830 years of seismic quiescence from palaeoseismology, archaeoseismology and historical seismicity along the Dead Sea fault in Syria, *Earth Planet. Sci. Lett.*, *210*, 35–52, doi:10.1016/S0012-821X(03)00144-4.

Nemer, T., M. Meghraoui, and K. Khair (2008), The Rachaya-Serghaya fault system (Lebanon): Evidence of coseismic ruptures, and the AD 1759 earthquake sequence, *J. Geophys. Res.*, *113*(B5), B05312, doi:10.1029/2007JB005090.

Niemi, T. M., H. Zhang, M. Atallah, and B. J. Harrison (2001), Late Pleistocene and Holocene slip rate of the Northern Wadi Araba fault Dead Sea Transform, Jordan, *J. Seismol.*, *5*, 449–474.

Overman, J. A. (2008), Horvat Omrit, in *The New Encyclopedia of Archaeological Excavations in the Holy Land*, vol. 5, edited by E. Stern, pp. 1987–1989, Carta, Jerusalem.

Politi, M. (2011), Branching of a continental transform in the Hula Basin: Subsurface evidence MSc (in Hebrew), The Hebrew Univ. of Jerusalem, 71 p.

Sadeh, M., Y. Hamiel, A. Ziv, Y. Bock, P. Fang, and S. Wdowinski (2012), Crustal deformation along the Dead Sea Transform and the Carmel Fault inferred from 12 years of GPS measurements, *J. Geophys. Res.*, *117*(B8), B08410, doi:10.1029/2012JB009241.

Savage, J. C., and R. O. Burford (1973), Geodetic Determination of Relative Plate Motion in Central California, *J. Geophys. Res.*, *78*(5), 832–845, doi:10.1029/JB078i005p00832.

Sbeinati, M. R., R. Darawcheh, and M. Mouty (2005), The historical earthquakes of Syria: An analysis of large and moderate earthquakes from 1365 B.C. to 1900 A.D, *Ann. Geophys.*, *48*(3), 347–435.

Schattner, U., and R. Weinberger (2008), A mid-Pleistocene deformation transition in the Hula basin, northern Israel: Implications for the tectonic evolution of the Dead Sea Fault, *Geochem. Geophys. Geosyst.*, *9*, Q07009, doi:10.1029/2007GC001937.

Sieberg, A. (1932), Erdbebengeographie, in *Handbuch der Geophysik*, Band IV, pp. 527–1005, Borntraeger, Berlin.

Stoehr, G. W. (2011), The potential for earthquake damage to Temple II architecture at Roman Omrit, in *The Roman Temple Complex at Horvat Omrit: Interim Rep.*, edited by J. A. Overman and D. Schowalter, pp. 85–100, BAR International Series, Oxford.

Thomas, R., T. M. Niemi, and S. T. Parker (2007), Structural damage from earthquakes in the second-ninth centuries at the archaeological site of Aila in Aqaba Jordan, *Bull. Am. Sch. Orient. Res.*, *346*, 59–77.

Wechsler, N., T. K. Rockwell, Y. Klinger, P. Štěpančíková, M. Kanari, S. Marco, and A. Agnon (2014), A paleoseismic record of earthquakes for the Dead Sea Transform Fault between the first and seventh centuries CE: Nonperiodic behavior of a plate boundary fault, *Bull. Seismol. Soc. Am.*, *104*(3), 1329–1347.

Weldon, R., K. Scharer, T. Fumal, and G. Biasi (2004), Wrightwood and the earthquake cycle: What a long recurrence record tells us about how faults work, *Geol. Soc. Am.*, *14*(9), 4–10.

Wells, D. L., and K. J. Coppersmith (1994), New empirical relationships among magnitudes, rupture length, rupture width, rupture area, and surface displacement, *Bull. Seismol. Soc. Am.*, *84*(4), 974–1002.

Zielke, O., J. R. Arrowsmith, L. G. Ludwig, and S. O. Akçiz (2010), Slip in the 1857 and earlier large earthquakes along the Carrizo Plain San Andreas Fault, *Science*, *327*(5969), 1119–1122.